Tailoring accessibility and amphiphilicity in MWW zeolites for the two-phase glycerol ketalization

Diego Lima, Laura Silva, Iago Zapelini, Svetlana Mintova, Leandro Martins

ARTICLE

Tailoring accessibility and amphiphilicity in MWW zeolites for the two-phase glycerol ketalization

Diego S. D. Lima[a], Laura L. Silva[a], Iago W. Zapelini[b], Svetlana Mintova[b], Leandro Martins[a]*

Two sets of MWW zeolite catalysts, the purely microporous MCM-22 (3D) and hierarchical ITQ-2 (2D), were synthesized and functionalized with an organosilane (?). These functionalized zeolites were employed in a two-phase glycerol ketalization reaction with acetone, eliminating the need for an additional solvent. There are two crucial factors to consider in this reaction: (i) the kinetic diameter of glycerol is comparable to the size of catalyst pores, limiting accessibility to the active sites, and (ii) glycerol exhibits poor solubility in acetone, causing the reaction to predominantly occur at the interfaces. Therefore, it is essential to focus on enhancing the accessibility of chemicals to the inner catalyst pores and adjusting the hydrophilic-hydrophobic balance of the functionalized catalysts to improve the reaction performance. The accessibility of the catalysts was indirectly evaluated by chemisorption of pyridine and 2,6-di-tert-butyl pyridine, which confirmed that ITQ-2 had a superior capacity to accommodate bulkier chemicals. Moreover, contact angle measurements of glycerol on ITQ-2 zeolites indicated that the functionalized materials exhibited reduced interaction with glycerol due to their increased hydrophobic nature. As a result, the functionalized materials tended to accumulate in the interfacial region, facilitating the dispersion of glycerol droplets within the reaction medium. However, the hydrophobic characteristics played a more significant role at the beginning of the reaction since, after reaching 25% conversion, the system transitioned into a single phase as the product itself acted as a solvent.

Introduction

Zeolites are essential to convert bio-derived products to fuels, chemicals, and materials in the context of biomass valorization. Their potential is highlighted by the many catalytic routes of biomass transformation they can promote based on their acid sites (Brønsted and Lewis), microporous attributes, and shape-selective properties.[1–4] However, the structural characteristics of bio-derivate compounds, such as bulky molecules and high O/C molar ratio, create two principal challenges to be overcome: (1) the intrinsic microporosity of zeolites that hampers diffusion of chemicals; (2) the issue of chemicals in liquid-phase reactions, which can lead to the formation of two phases, reducing the contact between the reactants, or solvate the active sites of the zeolites, decreasing the catalyst activity.

The major biomass compounds present high molecular weight, from 10^3 to 10^7 $g.mol^{-1}$.[3] Therefore, the strict microporosity of zeolites hinders bulky molecules' input, diffusion, and output, leading to low catalytic activity. In addition, the catalyst tends to deactivate more quickly due to coke formation in cavities.[1,4]

In response to the question of diffusion, studies have investigated improving zeolite accessibility by creating a second level of porosity (meso- or macropores) while preserving the intrinsic micropores.[1,2] The strategies include bottom-up methods, such as the addition of structure-directing agents in synthesis,[5,6] and top-down methods, such as desilication,[7] dealumination,[8,9] and delamination.[10]

The 2D ITQ-2 is delaminated hierarchical zeolites[4]. It was first synthesized by Corma *et al*.[11] in 1998 through a delamination of the MWW precursor, MCM-22(P). Due to layers condensation, the MCM-22(P) under calcination generates the traditional 3D zeolite MCM-22. Otherwise, the MCM-22(P) might have the layers swollen and further delaminated through the delamination method, resulting in the 2D material with disorganized layers and preserved MWW topology. The random distribution of layers creates mesoporous regions and maximizes the external area. Even with the loss of acidity due to the aggressive chemical treatment, the 2D material presents more accessible acid sites for bulky molecules to diffuse than the 3D structure.[12,13] It was used in biomass valorization reactions such as the alkylation of aromatics with 5-hydroxymethylfurfural (HMF),[14] ketalization of glycerol with HMF,[10] and glycerol dehydration.[15]

Regarding the issue of liquid-phase reactions in the processing of biomass chemicals, the solvents, especially water, tend to weaken the strength of acid sites through coordination and/or deprotonation.[3,16] Furthermore, water above 150 °C hydrolyzes the framework, leading to structural collapse.[3,17] Thus numerous studies have pointed on possible functionalization of zeolites with organosilanes have been performed.[18–21] The strategy lies in the organosilane anchoring on the zeolitic external surface by a silylation reaction, which improves the hydrophobic character of the catalyst,[22,23] expelling water molecules and favoring the material dispersion in non-polar media.[19,21] Considering the wide variety of bio-

derivates that present polar and non-polar groups, the functionalization of zeolites is a powerful technique to adjust the hydrophilic-hydrophobic character of the zeolite as desired. Furthermore, it enables more structural resistance of the catalyst in aqueous hot media.[17,24]

Ketalization of glycerol catalyzed by zeolites is an example of a reaction that faces the two highlighted obstacles: the reactants (glycerol and acetone) and products (solketal and dioxane) have limited diffusion in zeolite micropores, and water is a subproduct of the reaction that solvates the sites lessening the acid strength. Furthermore, glycerol presents a low solubility in the acetone phase of only 5 wt. %,[21] forming a two-phase system that prevents contact between the reactants. Consequently, the reaction only occurs at the interface between the phases, where the reactants interact.[25] A common alternative to overcome that limitation is the addition of a solvent,[26] but it would increase the complexity of the reaction medium.

In the solvent-free context, Nur, Ikeda, and Ohtani[27–29] presented the "Phase-Boundary Catalysis (PBC)" concept, which consists of the surface modification of the catalyst by organosilanes with the perspective of creating hydrophilic and hydrophobic regions. Due to its amphiphilic character, the material tends to place in the liquid-liquid interfacial region (boundary), enabling its active sites to be more accessible for the reactants while the system is vigorously stirred. According to the authors, PBC distinguishes from "Phase Transfer Catalysis" and "Pickering Interfacial Catalysis" since the catalyst does not transfer the reactants between the phases, and a stable emulsion is not formed.[30,31]

Herein we combined improved accessibility and functionalization of MWW zeolite catalysts (MCM-22 and ITQ-2) and applied them in the two-phase ketalization of glycerol with acetone.

Experimental

Synthesis of the MCM-22(P) precursor and MCM-22

First, 2.65 g of sodium hydroxide (NaOH, Sigma-Aldrich, > 98 wt.%) was added to 179.10 g of deionized H_2O under magnetic stirring until complete dissolution, followed by the addition of 2.12 g of sodium aluminate ($NaAl_2O_3$, Sigma-Aldrich, > 99%). Next, the synthesis mixture was heated to 50 °C, and 32.91 g of hexamethyleneimine (HMI, Sigma-Aldrich > 99 wt.%) under room temperature was added dropwise, keeping a constant vigorous mechanical stirring for 30 min. Finally, 33.23 g of fumed silica (SiO_2, 200 $m^2.g^{-1}$) was added slowly for 30 min in the synthesis mixture (50 °C), followed by an additional 30 min of agitation under the same conditions to complete homogenization. The molar composition of the final reaction mixture for synthesizing the MCM-22(P) precursor was 50 SiO_2: 1 $NaAl_2O_3$: 6 NaOH: 30 HMI: 900 H_2O. The synthesis procedure was based on the one described by Rodrigues et al.[15] The vessel was covered with parafilm to prevent mass loss by evaporation. The resulting mixture was transferred to five Teflon-coated autoclaves (50 mL) and kept at 150 °C for 9 days under static and autogenous conditions. The resulting material was washed several times with deionized water and centrifuged at 6000 rpm for 10 min until reaching a pH below 10.

To obtain the microporous MCM-22 in the protonic form, the MCM-22(P) precursor was dried at 60 °C for 24 h and then calcined in air at 550 °C for 3 h with a heating ramp of 2 °C.min^{-1}. Next, MCM-22 was ion-exchanged three times with a 0.1 mol.L^{-1} NH_4NO_3 aqueous solution, followed by washing and centrifugation at 6000 rpm for 10 min after each ion exchange cycle. Finally, the sample was calcined at 500 °C for 3 h using a heating ramp of 5 °C.min^{-1}, resulting in the protonic form of zeolite MCM-22.

Synthesis of ITQ-2 zeolite

The precursor zeolite MCM-22(P), still wet, was initially subjected to a swelling process according to the procedure established by Corma *et al*.[11] First, 9.8 g of MCM-22(P) and 55.4 g of hexadecyltrimethylammonium bromide (CTABr, Sigma-Aldrich, > 99%) were added to 190.9 g of deionized water, followed by 120.0 g of tetrapropylammonium hydroxide solution (TPAOH, Sigma-Aldrich, 20 wt. %). The mixture was refluxed at 80 °C for 24 h. The pH was 12.7 during the procedure. The flask was then immersed in an ultrasonic bath (Ultracleanner 1400A) at 50 °C and 40 kHz for 2 h to promote efficient delamination of the expanded zeolite. Then, hydrochloric acid (HCl, 37%) was added dropwise until the pH reached 2. Next, the mixture was washed with deionized water to remove the surfactant, centrifuged, and dried at 80 °C for 12 h. The dried material was calcined at 550 °C for 3 h with a heating rate of 2 °C.min^{-1} to remove the organic material. The previously calcined zeolites were converted into the protonic form after three consecutive ionic exchanges lasting 1 h each with 0.1 mol.L^{-1} NH_4NO_3 aqueous solution at room temperature and subsequent calcination at 500 °C for 3 h using a heating rate of 2 °C.min^{-1}.

Functionalization of the zeolites with dodecyltriethoxysilane

Functionalization of the protonic form of samples was performed with dodecyltriethoxysilane (Sigma-Aldrich, > 95%). The post-synthesis modification step was based on the procedure described by Zapelini and Cardoso,[32] Zapata et al.,[20] and Xu et al.[19] First, 1 g of the zeolite in the protonic form (MCM-22 or ITQ-2) was previously pre-treated at 130 °C under vacuum for 3 h to eliminate adsorbed water. Afterward, the material was stirred in 20 mL of anhydrous toluene and immersed in an ultrasonic bath for 1 h. Once a maximum dispersion of the material was guaranteed, 83.1 mg of dodecyltriethoxysilane was added to the system, equivalent to 83.2 µmol per gram of catalyst. The system was then stirred for 24 h under reflux at room temperature. Finally, the material was washed and centrifuged three times with 10 mL of ethanol and dried in an oven at 60 °C for 12 h. After the functionalization, the samples were labeled MCM-22 and ITQ-2, and MCM-22F and ITQ-2F.

Characterization of the catalysts

X-ray diffraction measurements of the powdered samples were performed in a Rigaku Model SmartLab, using Cu Kα radiation (40 kV, 15 mA) and 2θ acquisition range from 5 to 40° with a step size of 0.02° and goniometer speed of 2 °.min^{-1}. Scanning electron microscopy (SEM) was used to examine the formation of the samples' layers, crystal sizes, and morphologies. 0.050 mg of samples were previously dispersed in isopropyl alcohol and ultrasonicated for 30 min. Droplets of the dispersion were deposited onto an aluminum sample holder and analyzed in a FEI Magellan 400L microscope operated at 25 kV.

Nitrogen physisorption measurements at 77 K were performed in an ASAP 2010 Micromeritics instrument to determine the textural properties of the catalysts. Previously, 0.200 g of each sample was degassed, under vacuum, for 12 h at 250 °C. For the functionalized samples, the degassing temperature was 80 °C to prevent the desorption of organic groups. Micropore volume and the external area were calculated by the t-plot method. The mesopore volume was estimated by the difference between the micropore and the total pore volume at P/P_0 = 0.98. The adsorption branch was used to calculate pore size distribution by the BJH method.

Solid-state ^{27}Al MAS NMR was performed to investigate the aluminum species in the zeolite samples. The powdered samples were packed into 4 mm zirconia rotors. All the experiments were performed at 25 °C with a 10 kHz spinning rate. The spectra were collected in a Bruker Avance III 400 MHz equipped with a standard Bruker 4 mm magic-angle spinning (MAS) probe, operating at 104.21 MHz for ^{27}Al.

The acidity of the pristine zeolites was determined from measurements of ammonia desorption at a programmed temperature (NH_3-TPD). Previously, 200 mg of the zeolite in the H-form was pre-treatment at 400 °C, under a flow rate of 60 mL.min^{-1} of He for 1 h, followed by cooling to 100 °C. Then, the samples were subjected to a flow of pure helium for 2 h at 100 °C to remove the adsorbed ammonia. Finally, the ammonia molecules adsorbed on the acid sites were desorbed by heating the samples to 500 °C at a ramp of 10 °C.min^{-1} and monitored by a Pfeiffer Vacuum mass spectrometer connected to the reactor outlet.

Before functionalization, the samples' acidities were estimated by pyridine (Py) and 2,6-di-tert-butylpyridine (DTBPy) chemisorption monitored in situ by Fourier-Transform Infrared (FTIR) spectra recorded with a Thermo Scientific Nicolet iS50 FTIR spectrometer equipped with an MCT detector, at a spectral resolution of 4 cm^{-1}. Measurements were performed using self-supported disks of about 20 mg of powder. The samples were previously degassed at 450 °C for 4 h under a 10^{-5} Torr vacuum. The spectra of degassed samples were collected at room temperature and used for hydroxyl characterization and further subtraction after probe molecules adsorption. Probe molecules were delivered in the cell at room temperature (1 Torr for Py and 0.2 Torr for DTBPy),[33] followed by a treatment at 150 °C for 30 min for diffusion. The spectra of chemisorbed Py and DTBPy were acquired after the desorption step at 150 °C for 15 min under vacuum. The total concentration of the Brønsted (BAS) and Lewis (LAS) acid sites was calculated by integrating the peaks at approximately 1545 and 1454 cm^{-1}, raised in Py chemisorption experiments, with extinction coefficients of 1.72 for LAS and 1.30 cm.μmol^{-1} for BAS quantification by the Beer-Lambert equation.[34] The peak raised at around 1540 cm^{-1} in the DTBPy chemisorption experiment was used for external BAS (EBAS) quantification using the extinction coefficient of 1.30 cm.μmol-1.[35]

The functionalization of the zeolites with dodecyltriethoxysilane was confirmed by FTIR, using a Bruker Vertex 70 spectrometer equipped with a deuterated L-alanine-doped triglycine sulfate (DLaTGS) detector. The spectra were acquired from 2600 to 4000 cm^{-1} in transmittance mode using KBr pellets with 5 wt.% of zeolite.

The thermal behavior of the catalysts was studied using thermogravimetric analysis (TG) on TA Instruments DSC-TGA Q series 600 equipment. First, around 10 mg of the catalysts were loaded onto alumina pots and then allowed to equilibrate in 20 mL.min^{-1} of dry air flow. Next, the chamber was heated at a rate of 10 °C.min^{-1} to 100 °C, maintained for 1 h, and finally, heated up to 850 °C under dry air (20 mL.min^{-1}) and held for 30 min.

The hydrophobicity-hydrophilicity of the samples was measured by contact angle using a DataPhysics OCA equipment coupled with a CCD camera. The contact angle between the sample wafer (previously dried under vacuum overnight) and a 20 μL glycerol droplet was calculated based on the mean value of 3 measurements.

Catalytic test

The catalytic condensation reaction of glycerol with acetone (Equation 1) was carried out in a 2 mL batch microreactor. In a typical experiment, 200 mg of glycerol and 2.37 g of acetone (glycerol/acetone molar ratio of 1:6) were added to the reactor containing 20 mg of catalyst. The mixture was magnetically stirred for 5 to 80 min at 40 °C. The products were analyzed on a gas chromatograph (GC-2014, Shimadzu) equipped with a capillary column (Rtx-1, 30 m, 0.32 mm internal diameter, and 1 μm film thickness) and an FID detector. Before each injection, 0.09 g of n-butanol was added as an internal standard to carry out a quantitative mass balance of glycerol, acetone, and condensation products, solketal ((2,2-dimethyl-1, 3-dioxolan-4-yl) methanol) or dioxane (2,2-dimethyl-dioxan-5-ol). All products were confirmed using standards.

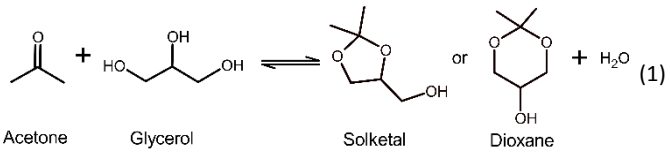

(1)

The initial turnover frequency, TOF_0, was calculated based on the glycerol conversion at time zero, allowing a more reliable comparison of the performance of different catalysts. The kinetic data were adjusted by Equation 2, where X (%) is the conversion and the time is t (in min). Parameters a and b were obtained from the least squares fitting, considering five conversion measures at different times (5, 10, 20, 40, and 80

min). Finally, the TOF_0 was calculated according to Equation 3, where N_0 corresponds to the moles of glycerol added to the reactor, and [BAS] the moles of Brønsted acid sites determined from Py-FTIR measurements.

$$X(\%) = \frac{a \cdot t}{b+t} \quad (2)$$

$$TOF_0 = \frac{N_0\left(\frac{dX(\%)}{dt}\right)_{t=0}}{[BAS].100} \quad (3)$$

Results and Discussion

Characterization of zeolite catalysts

Figure 1a shows the X-ray diffraction (XRD) patterns of the synthesized zeolites and the simulated pattern of the MWW structure for comparison. The non-calcined MCM-22(P) zeolite presents sharp and broad peaks, while the calcined MCM-22 exhibits sharper peaks due to the higher order of interconnected layers.[36] Both materials showed a similar patterns revealing the MWW topology. The most intense peak at 26.1° resembles the diffraction of the plane (301), whereas peaks in the 8-10° range correspond to (101) and (102) interlayer diffractions.[37,38] In the case of ITQ-2, the pattern is in good agreement with other studies.[11,15,39,40] The structure presents broad and low-intensity peaks that result from the long-range order reduction due to the exfoliation of layers during the alkaline treatment.[11,13] However, some peaks of MWW type, especially at 8.1 and 9.8°, indicate that the exfoliation was not complete, with a few stacked layers remaining.[40]

The SEM images shown in Figure 1b are in a good agreemet with the XRD results. The MCM-22 crystals show a rounded shape and organized layers. In contrast, the ITQ-2 layers are mostly irregularly distributed[40], preserving just few crystals resembling the typical MCM-22 morphology.

MCM-22 presents a type I isotherm based on N_2 physisorption measurments typical for purely microporous materials (Figure 1c). While the ITQ-2 catalyst showed a combination of type I and IV isotherms.[41] The hysteresis loop at relatively high pressure (P/P_0) is typical for disorganized ITQ-2 layers forming void spaces and slit-like pores in the mesopores region (between 8 and 34 nm). MCM-22 and ITQ-2 have micropore volumes of 0.133 and 0.099 $cm^3.g^{-1}$, and external areas of 42 and 229 $m^2.g^{-1}$, respectively. The lower microporosity of ITQ-2 is due to the delamination. The residual microporosity results from the remaining channels of the ten-membered rings (10 MR). The breakdown of the organized MCM-22 structure is responsible for the loss of microporosity, while 5 times increment in the external area is obtained resulting in more accesible surface and acid sites.

The BJH pore size distribution depicted in Figure 1d highlights the presence of mesopores with a broad distribution of pores between 4 to 38 nm. The wide range of pore-size families identified at 8.6, 16.3, and 34.9 nm arose from the nonselective nature of the chemical delamination. In contrast, the MCM-22 contains only micropores.

The IR spectra of the dried samples in the OH region (3900-3400 cm^{-1}) are shown in Figure 2a. The band at 3620 cm^{-1} is attributed to Brønsted acid sites, while the one at 3746 cm^{-1} refers to isolated silanol groups. Notably, the intensity of the peak at 3620 cm^{-1} decreases, implying a loss of acidic sites in the ITQ-2 sample.[12] At the same time, the intensity of the bands associated with the presence of silanols intensed due to the exfoliated layers. Finally, a broad and low-intense band at 3669 cm^{-1} refering to hydroxyl groups bonded to extra-framework aluminum is measured.

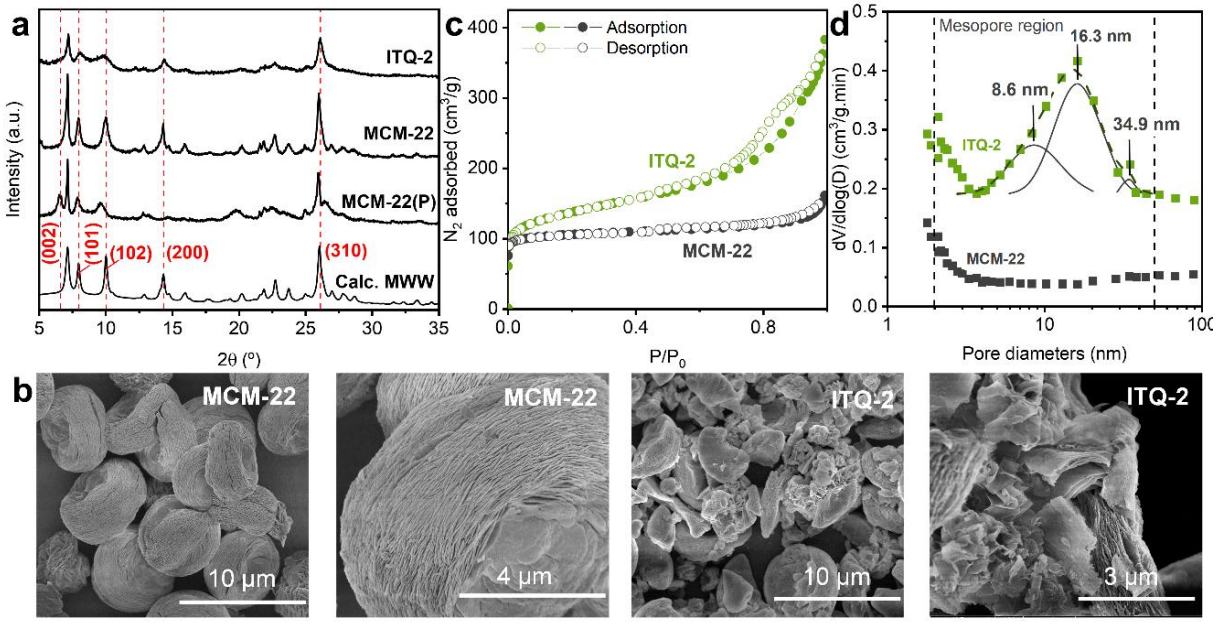

Fig. 1 (a) X-ray patterns of MWW samples, (b) scanning electron microscopy images, (c) N_2 physisorption isotherms, and (d) BJH pore size distribution (adsorption branch of the isotherms) of samples ???????.

Two distinct aluminum environments in the samples were observed in ^{27}Al NMR spectra (Figure 2b). The peak at 54 ppm is due to the presence of tetrahedral aluminum species in the zeolite framework. While the peak at 0 ppm relates the extra-framework hexacoordinated aluminum species.[6,42,43] The lower intensity of both peaks and greater width of the peak at 0 ppm indicate that the acid treatment promoted alteration in the coordination of aluminum atoms due to dealumination during exfoliation. The relative ratio of the peaks at 54 and 0 ppm are 6.4 and 5.3 for MCM-22 and ITQ-2, respectively. The lower ratio for ITQ-2 follows the loss of framework aluminum.[40] Additionally, the broadening of peak 2 in ITQ-2 (from -20 to 0 ppm) is a consequence of oligomeric aluminum species with different sizes and/or ionic species charge balancing the zeolite structure.[43]

TPD-NH3 and FTIR-pyridine results in Table 1 allowed quantifying the number of acid sites in MCM-22 and ITQ-2 samples, whereas FTIR-DTBPy quantified the external acid sites. MCM-22 had more acid sites than ITQ-2.[13,44] On the other hand, ITQ-2 had more Lewis acid sites (LAS) compared to MCM-22, which is related to the higher amount of aluminum in octahedral coordination (Figure 2b). The inferior quantification given by FTIR-Py compared to TPD-NH3 is due to the higher kinetic diameter of the pyridine molecule compared to ammonia. Table 2 shows that Pyridine has comparable dimension with the micropores that hinders the accessibility to the internal acid sites.[6]

Regarding the quantification of acid sites by 2,6-ditertbutyl-pyridine (DTBPy), the higher value obtained for ITQ-2 demonstrates the improvement in the accessibility of the catalyst, as the kinetic diameter of the DTBPy enables preferential adsorption on external sites or into pores higher than 1 nm. Additionally, the EBAS/BAS ratio gives the proportion of accessible sites for the bulky molecule for total Brønsted acidity, where the values suggest the ITQ-2 accessibility is higher three times than that of MCM-22.

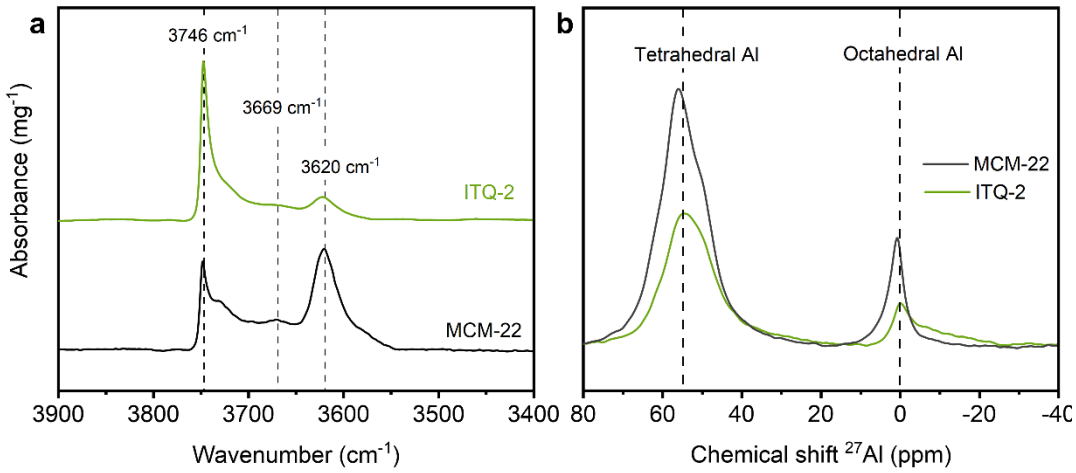

Fig. 2 (a) Infrared spectra of the vacuum-dried samples in the region 3400-3900 cm-1, and (b) ^{27}Al NMR spectra of samples ??????.

	TPD-NH_3 (µmol $NH_3 \cdot g^{-1}$)		FTIR - Py (µmol·g^{-1})		FTIR -DTBPy (µmol·g^{-1})	mole ratio
				Lewis sites (LAS)		
Catalysts	LT[a] 170-290ºC	HT[b] 290-500ºC	Brønsted sites (BAS)		External BAS (EBAS)	EBAS / BAS

[a] low-temperature peak and [b] high-temperature peak

Table 1 Quantification of acidic sites by TPD-NH3, FTIR-Py, and -DTBP ana

Table 2 Kinetic diameter of probe molecules and reactional compounds; diameter of pores of MCM-22 and ITQ-2.

ammonia[a]	190	0.38	378	203	248	27	0.13
pyridine[a]		0.54		**MCM-22**	0.40 x 0.50 0.40 x 0.55		…
DTBPy[b]		1.05					
glycerol[c]		0.54					8.6
acetone[c]		0.51		**ITQ-2**	0.40 x 0.50		16.3
solketal[c]		0.61					34.9

[a] Rodrigues *et al*. (2019)[6], [b] Song *et al*. (2005)[45], [c] Catuzo *et al*. (2020)[51], [d] Pergher and Schwanke (2018)[56] and [e] BJH

Characterization of functionalized zeolite catalysts

The functionalized zeolites were characterized by FTIR spectra (Figure 3a). The IR spectra of samples MCM-22F and ITQ-2F contain bands in the 2850-3000 cm^{-1} region, associated with the C-H stretching that are absent in the pristine samples.[19,23,24] The most intense band at 2930 cm^{-1} corresponds to vibrating modes of methyl groups (CH_2) of the long chain silane groups, whereas the bands at 2861 and 2976 cm^{-1} are attributed to terminal CH_3 stretches.[20,45] The band in the range 3290-3690 cm^{-1} corresponds to stretches of O-H groups of adsorbed water; the MCM-22F and ITQ-2F had a less intense band than non-functionalized samples, indicating that the treated materials had lower water adsorption.[46] Additionally the thermogravimetric analysis (TGA) provided information about the dodecylthrietoxisilane functionalized samples (Figure 3b). The TG curve shows an abrupt weight loss from 115 to 300 °C, resembling the organosilane removal. Yamazaki *et al.*[47] reported two temperature stages at 115 - 220 °C, corresponding to silane monomers vaporization, and at 220 - 300 °C, related to silane oligomers vaporization. In the course of the TGA analysis, the monomers tend to condensate to each other under increasing of the temperature, producing oligomeric species.

Regarding the functionalized and pristine samples (Figure 3c), the weight variance at *ca*. 650 °C confirmed the degradation of anchored organosilanes. When analyzing the region from 100 to 180 °C for both MCM-22 and ITQ-2 samples, there is a significant difference in the water adsorption capacity, i.e. of 1.7 % and 2.6 %, respectively. The greater affinity of the ITQ-2 sample for the organosilane is due to the presence of higer amount of SiOH groups generated after the chemical treatment.

After water removal, the MCM-22 and ITQ-2 lost weight only through dehydroxylation until 850 °C. In comparison, the functionalized materials keep losing mass dur to the organosilane vaporization until 300 °C: 2.06 % for MCM-22F and 1.59 % for ITQ-2. Yamazaki *et al.*[47] and Builes *et al.*[48] attribute that stage to the desorption of organosilane adsorbed on the zeolite surface. While the anchored organosilanes degradation started at 300 °C and finished at 650 °C. The temperature deviation of these stages agree with other works.[20,21,48]

As expected, the functionalization has not modified the material structure. However, anchoring the organic compounds on the external surface caused losses in the microporosity of MCM-22F and ITQ-2F samples due to the pore entrance blockage (Figure 3d and Table 3). The loss in microporosity was 39 % and 50 % for MCM-22F and ITQ-2F, respectively. Similar results have been reported earlier.[21,22,46,49] Builes *et al.*[48] reported that the organic compound can block the pores entrance in two ways: (i) formation of oligomers by condensation of mono or dicoordinated species or (ii) formation of a barrier by laterals alkoxides of monomers species, as exemplified in Figure 3d. As a result, both the micropore and mesopore volumes of the samples decreased. The blockage entrance also occurred in mesopores but in a lower proportion, only ~6 % of the mesoporous volume was lost.[48] The external surface of the catalysts was not affected.

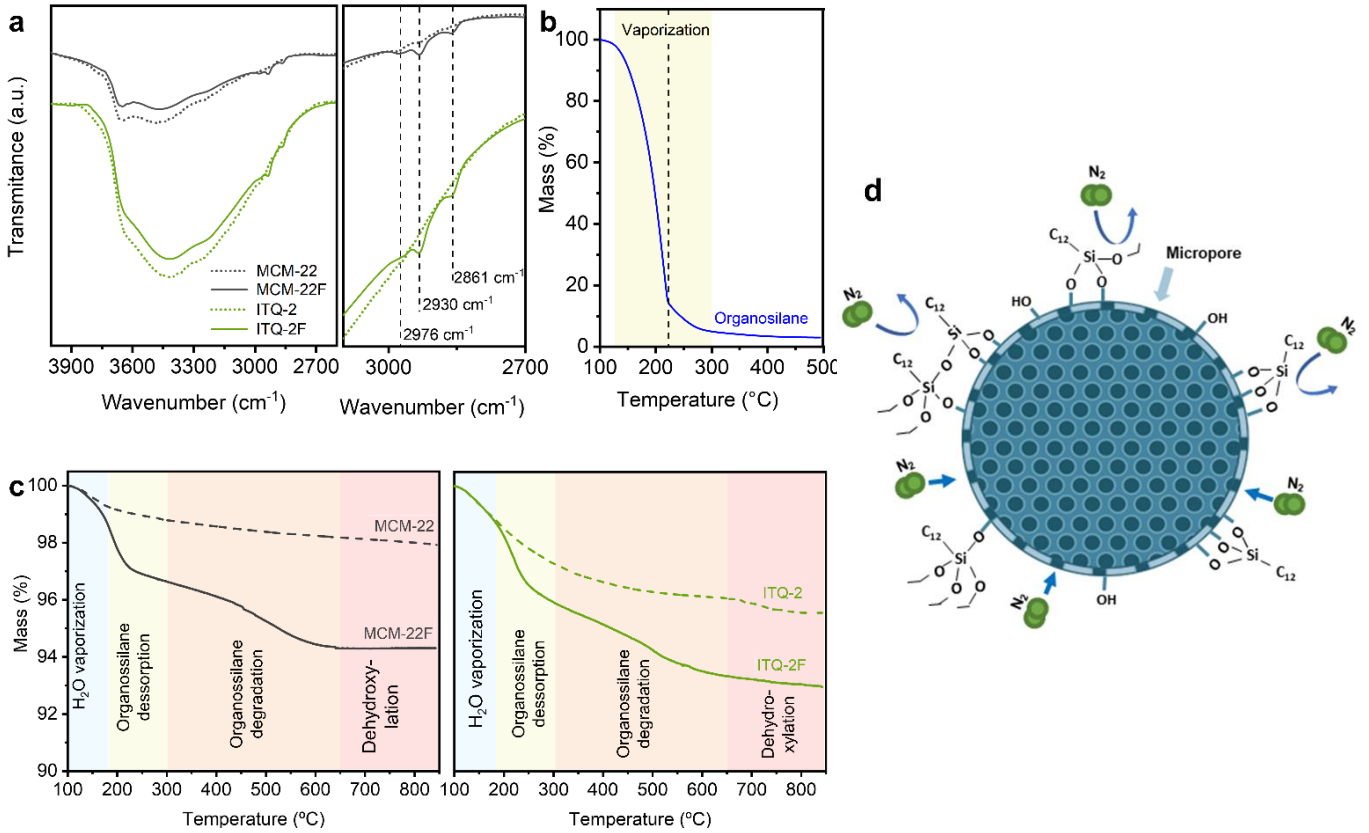

Fig. 3 (a) FTIR spectra of samples MCM-22, MCM-22F, ITQ-2, and ITQ-2F, (b) TG curve of pure dodecylthrietoxisilane in the range of 100 - 500 ºC, (c) TG curves of samples MCM-22, MCM-22F, ITQ-2 and ITQ-2F in the range of 100 – 850 ºC. (d) Scheme representation showing possible encoring of the dodecylthrietoxisilane on the zeolite catalysts.

Table 3 Quantitative results obtained for parent and functionalized zeolite catalysts based on N_2 physisorption measurments.

Catalysts	Micropore volume ($cm^3.g^{-1}$) / lost V_{mic}	Mesopore volume ($cm^3.g^{-1}$) / lost V_{mes}	External area ($m^2.g^{-1}$) / lost area
MCM-22	0.13	0	42.1
MCM-22F	0.08 / (-39 %)	0	41.7 / (-1 %)
ITQ-2	0.10	0.29	229.2
ITQ-2F	0.05 / (-50 %)	0.27 / (-6 %)	223.6 / (-2 %)

Catalytic tests

The strong interaction between glycerol-glycerol (G/G) through hydrogen bonds prevents the glycerol-acetone (G/A) interactions, leading to a two-phase system.[25] Therefore the reaction occurs preferentially in the interphase region, where there are G/A interactions. Otherwise, the solketal product presents a surfactant character, facilitating contact between the reactants. Rahaman *et al*.[21] have discovered that after 25 % of solketal formation, the system gradually becomes homogeneous, and the G/A interaction is maximized. Increasing temperature improves the G/A interaction during the heterogeneous step of the system but, conversely, decreases the equilibrium conversion due to the exothermic character of the reaction.[50] In that perspective, the reaction was conducted at a low temperature (40 °C) using a 6:1 molar proportion of acetone/glycerol. As a result, the equilibrium conversion is estimated at 78 % at that condition.[51]

As exposed in Scheme 1 and discussed by Calvino-Casilda *et al*.[25] and Venkatesha *et al*.,[8] the ketalization occurs via BAS and LAS.[52] Although both sites can participate, studies point out that Brønsted acid sites are more favorable for the reaction.[25] After the protonation (via BAS) or anchoring (via LAS) of acetone, the glycerol molecule promotes nucleophilic attack to the carbonyl acetone forming the intermediate hemiacetal, which is highly unstable[51]. The intermediate is then led to the cyclization step, producing ketals of five- or six-membered rings, 2,2- dimethyl-1,3-dioxolan-4-yl methanol (solketal) or 2,2-dimethyl-1,3-dioxan-5-ol (dioxane), respectively. The formation of the cyclic ketals is considered as the rate-determining step due to transition state destabilization and hydrolysis reverse-reaction. The solketal can be obtained by direct cyclization or by dioxane rearrangement.

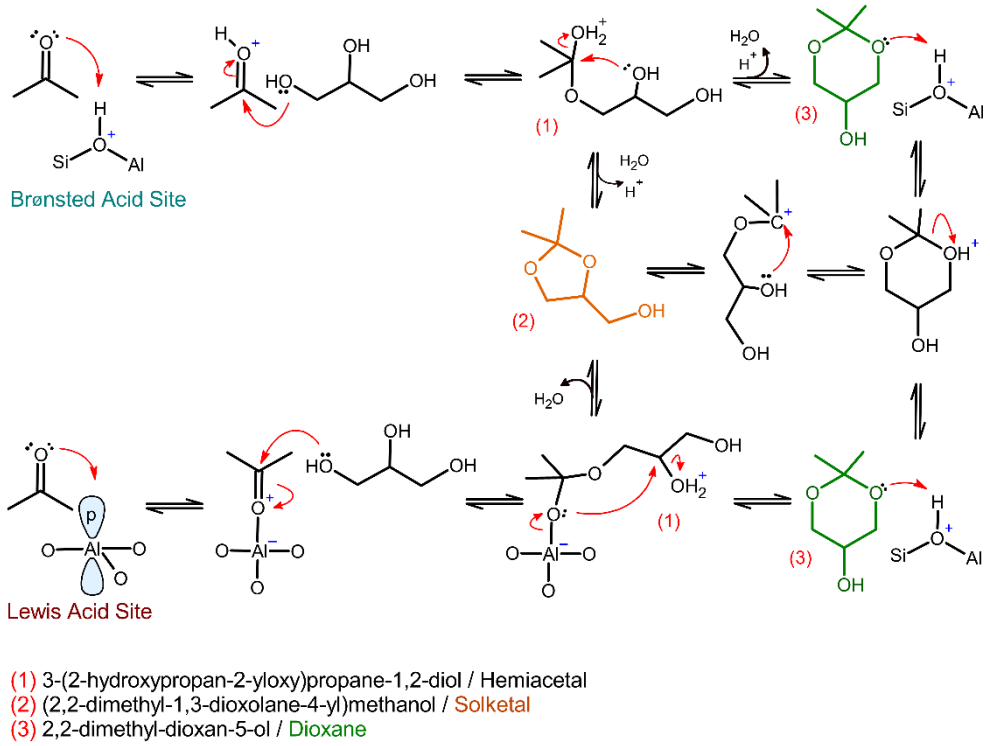

Scheme 1 Solketal selectivity obtained herein compared with other studies for reactions conducted at 40 ºC.

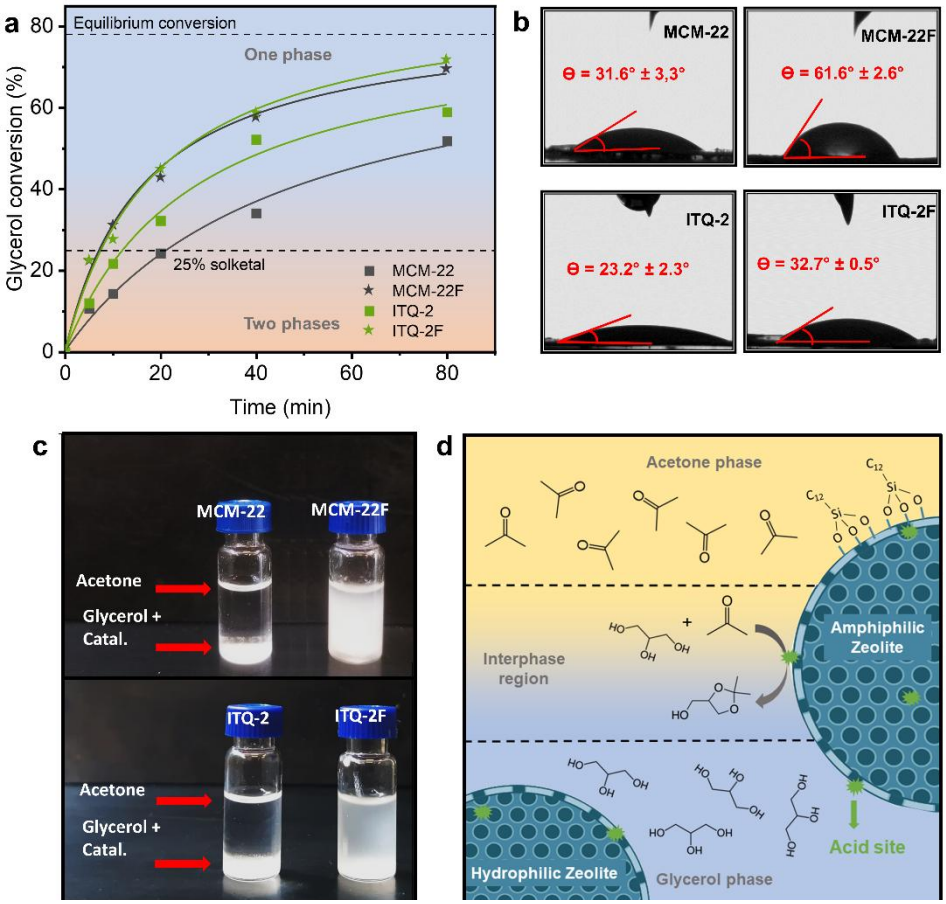

Fig. 4 (a) Glycerol conversion using MCM-22, MCM-22P, ITQ-2, and ITQ-2F catalysts up to 80 min, (b) glycerol contact angle for the catalysts, (c) photographs of the reaction system after 10 s of agitation and 30 s in rest stopped, indicating the formation of two phases using the MCM-22 and ITQ-2 catalysts, and (d) schematic representtion for the distribution of the catalysts in the two-phase system

The glycerol conversion as a function of time for the four studied catalysts is presented in Figure 4a. Considering that MCM-22 gives the highest number of total acid sites and the reaction is faster on Brønsted acid sites than on Lewis's,[25] it would be plausible to assume that the MCM-22 is more active than ITQ-2. However, the results of glycerol conversion as a function of time contest that consideration. The diameter of molecules involved in the reaction and the sizes of catalysts pores are presented in Table 2. For example, the glycerol and acetone have similar dimensions with the 10MR pores of the MCM-22, while the bulky ketals (0.61 nm) are larger. It prevents the internal diffusion of chemicals, intermediates stabilization, and the diffision of products from the channels. Therefore, it is reasonable to consider that the reaction occurs preferably on the external surface of the microporous zeolite.

The ITQ-2 has higher external surface area and mesopores allowing free diffusion of chemicals and more accessible acid sites. Furthermore, Maksimov *et al.*[52] highlight that the confinement effect of the hemiacetal specie during the cyclization step provided by the mesopores of the catalyst is essential for stabilizing the transition state. These two aspects justify the superior activity of ITQ-2. In agreement with those results, Arias *et al.*[10] have recently shown the ITQ-2 mesopores were responsible for the high yield of 5-hydroxymethylfurfural ketalization compared to zeolites Beta and HY, and MCM-41, which proves the importance of the balance of acidity and accessibility.

Figure 4b shows the contact angle measurements of the catalysts. ITQ-2 had a lower contact angle than MCM-22, due to the presence of hydrophilic silanol groups within the layers that improve water adsorption. These results are consistent with the hydrophilicity of the samples determined based on TG and FTIR analyses (Figure 3). A strong hydrophilic character of the catalyst is disadvantageous for the ketalization of glycerol since the water is a byproduct of the reaction. Its presence accelerates the reverse reaction and hinders the acidity due to the solvation of the active sites.[51,53,54] Given this, ITQ-2 is the most prone catalyst for water absorption. However, its superior performance denotes that accessibility, stabilization of intermediates, and internal diffusion of chemicals play more important role than the hydrophilicity in this reaction. Both catalysts MCM-22F and ITQ-2F showed similar high glycerol conversion and superior performance to the unmodified zeolites (see Figures 4b and 4c). The glycerol contact angle for the functionalized zeolites increased as can be seen in Figure 4b. Although none of the functionalized materials became completely hydrophobic, the variation in the contact angles caused by the presence of the organosilane confirms the

decrease in the hydrophilicity. The MCM-22F showed an increase of the contact angle by 30°, whereas for the ITQ-2 increased by 9.5°. This difference indicates that the silanol excess in the ITQ-2 surface minimizes the hydrophobic effect caused by the organosilane. The reaction system containing the catalysts after agitation for 10 s followed by 30 s resting is presented in Figure 4c. This results confirm that the functionalized catalysts can be dispersed throughout the reaction system due to the presence of organosilane. At the same time, the MCM-22 and ITQ-2 materials tend to precipitate at the bottom of the reactor due to gravity and affinity to glycerol.

In agreement with the "Phase-Boundary Catalysis" model proposed by Nur, Ikeda, and Ohtani,[28] the amphiphilic character of the functionalized catalysts enables their presence in interphase regions, interacting with both phases of the system. Considering the presence of accessible acid sites and G/A interactions in that region, the reaction occurs more easily,[27,29] while in the pure catalysts systems, the MCM-22 and ITQ-2 particles are in the glycerol phase. Therefore, the amphiphilic character of the catalysts is important in placing them in the interphase. Furthermore, the reduction of hydrophilicity minimizes the presence of water molecules nearby catalyst acid sites, conserving the strength of acid sites available to conduct the reaction.[19,20]

The TOF_0 (turnover frequency at time zero) of the catalysts (Figure 5a) was calculated using the experimental data of the glycerol conversion (Figure 4a), divided by the number of acid sites determined for the catalysts by FTIR-Py. The ITQ-2 showed a TOF_0 two times higher than MCM-22 due to accessibilitys improvement. At the same time, MCM-22 and ITQ-2 presented lower TOF0 than the functionalized catalysts due to their increased hydrophobicity. The ITQ-2F was the most efficient catalyst due to the contributions from the hierarchical structure and attenuation of water interaction due to functionalization. A relationship between the TOF and glycerol contact angle is observed (Figure 5a). The hierarchical ITQ-2 had a slope two times superior to that of the microporous MCM-22. It shows that the increase of hydrophobicity was more important for ITQ-2 than for the MCM-22. It reflects the tendency of ITQ-2 to adsorb water, associated with the high number of terminal silanols, leading to the inhibition of acid sites by water molecules. Thus, ITQ-2 was the catalyst that mostly benefited from the functionalization.

For solketal formation above 25 % glycerol conversion, new TOF values were calculated representing the reaction at that stage (Figure 5b), named $TOF_{25\%}$. As expected, all materials had decreased TOF values due to the diminishing concentration of reactants. A decrese of the slopes relative to that shown in Figure 5a is observed which is associated with the change of glycerol solubility in the reaction mixture. As long as the system is immiscible, MCM-22 and ITQ-2 are limited in the glycerol phase, while MCM-22F and ITQ-2F are more activly participating in the interphase reaction. However, considering the co-solvent effect of solketal, the system gradually becomes miscible after ~25 % formation,[21] leading to termination of the separation of phases. Thus, the non-functionalized catalysts have full contact with the chemicals. The finding demonstrates the importance of functionalization in the reaction onset. As the reaction progresses, the significance of the amphiphilicity decreases.

In general, all materials tended to increase solketal selectivity as a function of time, which can be explained by the superior stability of solketal over its isomer (Figure 5c). In addition, the steric repulsion between the methyl groups in the axial position for the six-membered ring destabilizes the dioxane compound and favors its rearrangement for solketal (Scheme 1).[26] Besides, it can be seen that MCM-22F, ITQ-2F, and ITQ-2 present similar highest selectivity at 80 min (~ 97.7 %). According to Scheme 1, dioxane is converted to solketal by reaction with the Brønsted acid sites, further promoting rearrangement and solketal formation. Since ITQ-2 and ITQ-2F have many acid sites and mesopores available for the diffusion of large dioxanes and stabilization of the transition state, converting dioxane to solketal is favorable, as previously reported [6,8]. Concerning MCM-22F, the high selectivity may be explained by the minor water adsorption on the surface due to its higher hydrophobicity resulting in more favorable rearrangement of dioxane than its hydrolysis[8,25]. Other studies have reported similar selectivity results to those reported here at 40 °C, as shown in Table 3.

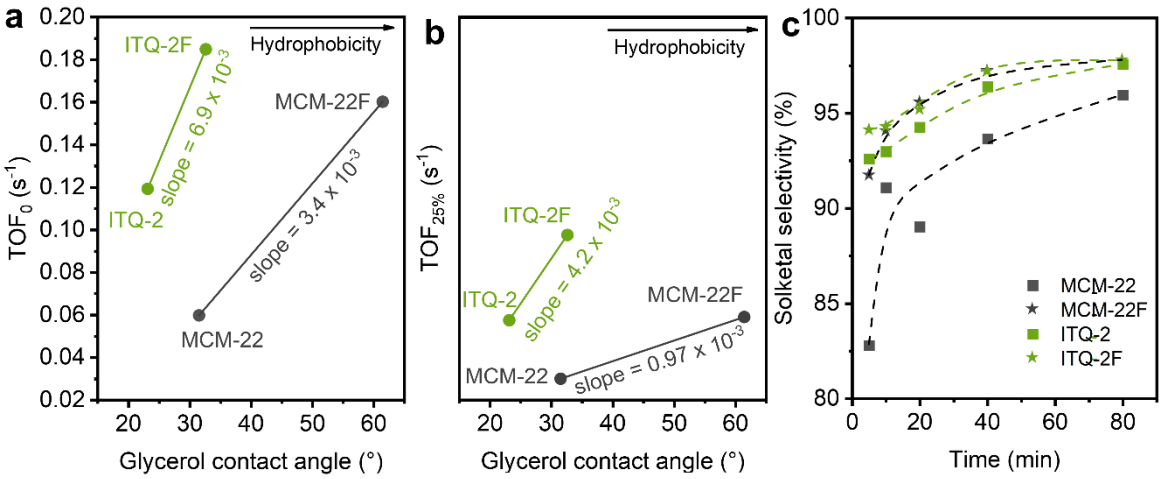

Fig. 5 (a) TOF0 values for the MCM-22, MCM-22F, ITQ-2, and ITQ-2F, (b) TOF values estimated at 25 % of solketal selectivity, and (c) solketal selectivity along the reaction time.

Table 4 Solketal selectivity obtained herein compared with other studies conducted at 40 ºC.

Authors	Catalyst	Time (min)	Conv. (%)	Solketal selectivity (%)
Catuzo, Santilli, Martins[51]	ZSM-5 (Si/Al = 140)	100	51	98
Rodrigues *et al*.[6]	Hierarchical MCM-22	80	70	98
Fan *et al*.[55]	TiO_2-SiO_2	180	78	75
Calvino-Cacilda *et al*.[25]	Niobium-modified mesoporous cellular foams	180	80	97
This work	ITQ-2F	80	70	98

Conclusions

In this study, we utilized the ketalization of glycerol with acetone to investigate the impact of accessibility and amphiphilicity achieved through zeolite delamination and functionalization, specifically focusing on MWW-type zeolites. The delaminated ITQ-2 zeolite exhibited enhanced accessibility for bulky molecules, resulting in higher catalytic activity compared to the purely microporous MCM-22 zeolite. Additionally, the ITQ-2 catalyst possessed a greater number of silanol groups due to the delamination process, leading to superior hydrophilicity.

Interestingly, the superior hydrophilicity did not negatively affect the catalysts' performance, suggesting that accessibility plays a more significant role than hydrophilicity in this particular reaction. The functionalized catalysts demonstrated improved catalytic performance compared to the pure catalysts due to the reduction in hydrophilicity. This reduction prevented water from solvating the acid sites, enabling the catalytic reactions to occur at the phase boundary.

Furthermore, functionalization played a crucial role in the catalysts' performance, as the reaction proceeded in a two-phase system. As the reaction progressed, the products solubilized both phases, resulting in a one-phase reaction mixture, and the functionalized and non-functionalized catalysts tended to minimize their differences.

Enhancing accessibility and adjusting the hydrophilic-hydrophobic balance are essential strategies for the application of zeolites in converting bulky chemicals within a biomass context. Moreover, our findings demonstrate that combining both approaches can effectively promote liquid-phase catalytic reactions using zeolite catalysts with predesigned properties.

Author Contributions

Diego S. D Lima: Conceptualization, Investigation, Data curation, Formal Analysis, Writing – original draft. **Laura. L. Silva:** Conceptualization, Supervision, Writing - review & editing. **Iago W. Zapelini:** Investigation, Formal analysis, Writing - review & editing. **Svetlana Mintova:** Resources, Writing - review & editing. **Leandro Martins:** Conceptualization, Funding acquisition, Resources, Writing - review & editing.

Conflicts of interest

There are no conflicts to declare.

Acknowledgements

The authors are grateful for the financial support granted by the São Paulo Research Foundation - FAPESP, grants #2017/21965-5, #2018/01258-5, #2021/08326-9, and #2022/01789-6. In addition, we acknowledge the GFQM/UNESP for the contact angle measurements and N_2 physisorption, and the LCE/UFSCar for the scanning electron microscopy images.

Notes and references

1 T. Ennaert, J. Van Aelst, J. Dijkmans, R. De Clercq, W. Schutyser, M. Dusselier, D. Verboekend and B. F. Sels, *Chem Soc Rev*, 2016, **45**, 584–611.

2 S. Mardiana, N. J. Azhari, T. Ilmi and G. T. M. Kadja, Hierarchical zeolite for biomass conversion to biofuel: A review, *Fue*l, 2022, DOI: 10.1016/j.fuel.2021.122119.

3 R. Rinaldi and F. Schüth, Design of solid catalysts for the conversion of biomass, *Energy Environ Sci*, 2009, **2**, 610–626.

4 J. Přech, P. Pizarro, D. P. Serrano and J. Áejka, From 3D to 2D zeolite catalytic materials, *Chem Soc Rev*, 2018, **47**, 8263–8306.

5 S. Kelkar, C. M. Saffron, Z. Li, S. S. Kim, T. J. Pinnavaia, D. J. Miller and R. Kriegel, Aromatics from biomass pyrolysis vapour using a bifunctional mesoporous catalyst, *Green Chemistry*, 2014, **16**, 803–812.

6 M. V Rodrigues, C. Okolie, C. Sievers and L. Martins, Organosilane-Assisted Synthesis of Hierarchical MCM-22 Zeolites for Condensation of Glycerol into Bulky Products, *Cryst Growth Des*, 2019, **19**, 231–241.

7 J. R. García, M. Bertero, M. Falco and U. Sedran, Catalytic cracking of bio-oils improved by the formation of mesopores by means of y zeolite desilication, *Appl Catal A Gen*, 2015, **503**, 1–8.

8 N. J. Venkatesha, Y. S. Bhat and B. S. Jai Prakash, Dealuminated BEA zeolite for selective synthesis of five-membered cyclic acetal from glycerol under ambient conditions, *RSC Adv*, 2016, **6**, 18824–18833.

9 P. Manjunathan, S. P. Maradur, A. B. Halgeri and G. V. Shanbhag, Room temperature synthesis of solketal from acetalization of glycerol with acetone: Effect of crystallite size and the role of acidity of beta zeolite, *J Mol Catal A Chem*, 2015, **396**, 47–54.

10 K. S. Arias, A. Garcia-Ortiz, M. J. Climent, A. Corma and S. Iborra, Mutual Valorization of 5-Hydroxymethylfurfural and Glycerol into Valuable Diol Monomers with Solid Acid Catalysts, *ACS Sustain Chem Eng*, 2018, **6**, 4239–4245.

11 A. Corma, V. Fornes, S. B. Pergher, T. L. M. Maesen and J. G. Buglass, Delaminated zeolite precursors as selective acidic catalysts, *Nature*, 1998, **396**, 353–356.

12 A. Corma, V. Fornes, J. Martinez-Triguero and S. B. Pergher, Delaminated zeolites: Combining the benefits of zeolites and mesoporous materials for catalytic uses, *J Catal*, 1999, **186**, 57–63.

13 A. Corma, V. Fornes, J. M. Guil, S. Pergher, T. L. M. Maesen and J. G. Buglass, Preparation, characterisation and catalytic activity of ITQ-2, a delaminated zeolite, *Microporous Mesoporous Mater.*, 2000, **38**, 301–309.

14 K. S. Arias, M. J. Climent, A. Corma and S. Iborra, Synthesis of high quality alkyl naphthenic kerosene by reacting an oil refinery with a biomass refinery stream, *Energy Environ Sci*, 2015, **8**, 317–331.

15 M. V Rodrigues, C. Vignatti, T. Garetto, S. H. Pulcinelli, C. V Santilli and L. Martins, Glycerol dehydration catalyzed by MWW zeolites and the changes in the catalyst deactivation caused by porosity modification, *Appl. Catal. A*, 2015, **495**, 84–91.

16 E. Grifoni, G. M. Piccini, J. A. Lercher, V. A. Glezakou, R. Rousseau and M. Parrinello, Confinement effects and acid strength in zeolites, *Nat. Commun.*, 2021, DOI:10.1038/s41467-021-22936-0.

17 P. A. Zapata, Y. Huang, M. A. Gonzalez-Borja and D. E. Resasco, Silylated hydrophobic zeolites with enhanced tolerance to hot liquid water, *J. Catal.*, 2013, **308**, 82–97.

18 F. Liu, K. Huang, A. Zheng, F. S. Xiao and S. Dai, Hydrophobic Solid Acids and Their Catalytic Applications in Green and Sustainable Chemistry, *ACS Catal.*, 2018, **8**, 372–391.

19 S. Xu, H. Sheng, T. Ye, D. Hu and S. Liao, Hydrophobic aluminosilicate zeolites as highly efficient catalysts for the dehydration of alcohols, *Catal. Commun.*, 2016, **78**, 75–79.

20 P. A. Zapata, J. Faria, M. P. Ruiz, R. E. Jentoft and D. E. Resasco, Hydrophobic Zeolites for Biofuel Upgrading Reactions at the Liquid-Liquid Interface in Water/Oil Emulsions, *J. Am. Chem. Soc.*, 2012, **134**, 8570–8578.

21 M. S. Rahaman, T. K. Phung, M. A. Hossain, E. Chowdhury, S. Tulaphol, S. B. Lalvani, M. O'Toole, G. A. Willing, J. B. Jasinski, M. Crocker and N. Sathitsuksanoh, Hydrophobic functionalization of HY zeolites for efficient conversion of glycerol to solketal, *Appl. Catal., A*, 2020, DOI: 10.1016/j.apcata.2019.117369.

22 T. Montanari, M. C. H. Delgado, M. Bevilacqua, G. Busca, M. Vargas and L. J. Alemany, Surface modification of H-ferrierite by reaction with triethoxysaline, *J. Phys. Chem. B*, 2005, **109**, 879–883.

23 L. Bonaccorsi, P. Bruzzaniti, L. Calabrese and E. Proverbio, Organosilanes functionalization of alumino-silica zeolites for water adsorption applications, *Microporous Mesoporous Mater.*, 2016, **234**, 113–119.

24 L. Zhang, B. Xue, T. Chen and G. Li, Silane functionalization on zeolite 13X surface for direct steam generation in a solid sorption heat pump, *Energy Convers. Manag.*, DOI: 10.1016/j.enconman.2021.114457.

25 V. Calvino-Casilda, K. Stawicka, M. Trejda, M. Ziolek and M. A. Bañares, Real-Time Raman monitoring and control of the catalytic acetalization of glycerol with acetone over modified mesoporous cellular foams, *J. Phys. Chem. C*, 2014, **118**, 10780–10791.

26 M. N. Moreira, R. P. V. Faria, A. M. Ribeiro and A. E. Rodrigues, Organosilane-Assisted Synthesis of Hierarchical MCM-22 Zeolites for Condensation of Glycerol into Bulky Products, *Ind. Eng. Chem. Res.*, 2019, **58**, 17746–17759.

27 H. Nur, S. Ikeda and B. Ohtani, Phase-boundary catalysis of alkene epoxidation with aqueous hydrogen peroxide using amphiphilic zeolite particles loaded with titanium oxide, *J. Catal.*, 2001, **204**, 402–408.

28 H. Nur, S. Ikeda and B. Ohtani, Phase-boundary catalysis: A new approach in alkene epoxidation with hydrogen peroxide by zeolite loaded with alkylsilane-covered titanium oxide, *Chem. Commun.*, 2000, 2235–2236.

29 H. Nur, S. Ikeda and B. Ohtani, Phase-Boundary Catalysts for Acid-Catalyzed Reactions: The Role of Bimodal Amphiphilic Structure and Location of Active Sites, *J. Braz. Chem. Soc.*, 2004, DOI: 10.1590/S0103-50532004000500018.

30 M. Pera-Titus, L. Leclercq, J.-M. Clacens, F. De Campo and V. Nardello-Rataj, Pickering Interfacial Catalysis for Biphasic Systems: From Emulsion Design to Green Reactions, *Angewandte Chemie-International Edition*, 2015, **54**, 2006–2021.

31 H. Nur, S. Ikeda and B. Ohtani, Amphiphilic NaY zeolite particles loaded with niobic acid: Materials with applications for catalysis in immiscible liquid-liquid system, *React. Kinet. Catal. Lett.*, 2004, **82**, 255–261.

32 I. W. Zapelini and D. Cardoso, Amine-grafted Na-LTA zeolite precursors as basic catalysts for Knoevenagel condensation, *Microporous Mesoporous Mater.*, 2021, DOI: 10.1016/j.micromeso.2021.111270.

33 L. Lakiss, A. Vicente, J.-P. Gilson, V. Valtchev, S. Mintova, A. Vimont, R. Bedard, S. Abdo and J. Bricker, Probing the

Bronsted Acidity of the External Surface of Faujasite-Type Zeolites, *Chemphyschem*, 2020, **21**, 1873–1881.

34 J. Datka, A. M. Turek, J. M. Jehng and I. E. Wachs, Acidic properties of supported niobium oxide catalysts – An Infrared-spectroscopy investigation, J. Catal., 1992, **135**, 186–199.

35 N. D. Shcherban, R. Y. Barakov, P. Maki-Arvela, S. A. Sergiienko, I. Bezverkhyy, K. Eranen and D. Y. Murzin, Isomerization of alpha-pinene oxide over ZSM-5 based micro-mesoporous materials, *Appl. Catal., A*, 2018, **560**, 236–247.

36 S. L. Lawton, A. S. Fung, G. J. Kennedy, L. B. Alemany, C. D. Chang, G. H. Hatzikos, D. N. Lissy, M. K. Rubin, H. K. C. Timken, S. Steuernagel and D. E. Woessner, Zeolite MCM-49: A three-dimensional MCM-22 analogue synthesized by in situ crystallization, *J. Phys. Chem*., 1996, **100**, 3788–3798.

37 V. J. Margarit, M. E. Martinez-Armero, M. T. Navarro, C. Martinez and A. Corma, *J. Phys. Chem*., *Angewandte Chemie-International Edition*, 2015, **54**, 13724–13728.

38 M. V Rodrigues, L. H. Vieira, G. P. Campos and L. Martins, Effect of different seed sources on the hydrothermal crystallization of MCM-22 zeolite catalysts, *CrystEngComm*, 2018, **20**, 3467–3475.

39 J. Hao, Y. Wang, G. Liu, J. Zhang, G. Li and X. Ma, Synthesis of ITQ-2 zeolites and catalytic performance in n-dodecane cracking, *Chin. J. Chem. Eng.*, 2014, **22**, 869–874.

40 G. Lee, E. Jang, T. Lee, Y. Jeong, H. Kim, S. Lee, Y. G. Chung, K.-S. Ha, H. Baik, H.-G. Jang, S. J. Cho and J. Choi, Effective delamination of a layered two-dimensional MCM-22 zeolite: Quantitative insights into the role of the delaminated structure on acid catalytic reactions*, Catal. Today*, 2023, DOI: 10.1016/j.cattod.2022.07.024.

41 M. Thommes, K. Kaneko, A. V. Neimark, J. P. Olivier, F. Rodriguez-Reinoso, J. Rouquerol and K. S. W. Sing, Physisorption of gases, with special reference to the evaluation of surface area and pore size distribution (IUPAC Technical Report), *Pure App. Chem.*, 2015**, 87**, 1051–1069.

42 Z. Yu, Q. Wang, L. Chen and F. Deng, Bronsted/Lewis Acid Sites Synergy in H-MCM-22 Zeolite Studied by H-1 and Al-27 DQ-MAS NMR Spectroscopy, *Chin. J. Catal*, 2012, **33**, 129–139.

43 L. G. Possato, R. N. Diniz, T. Garetto, S. H. Pulcinelli, C. V. Santilli and L. Martins, A comparative study of glycerol dehydration catalyzed by micro/mesoporous MFI zeolites, *J. Catal.,* 2013, **300**, 102–112.

44 A. Corma, U. Diaz, V. Fornes, J. M. Guil, J. Martinez-Triguero and E. J. Creyghton, Characterization and catalytic activity of MCM-22 and MCM-56 compared with ITQ-2, *J. Catal*, 2000, **191**, 218–224.

45 W. Song, J. F. Woodworth, V. H. Grassian and S. C. Larsen, Microscopic and macroscopic characterization of organosilane-functionalized nanocrystalline NaZSM-5, *Langmuir*, 2005, **21**, 7009–7014.

46 C. X. Yan, J. F. Ding, T. L. Ma, R. Shao, W. Xu, J. He and P. F. Wang, Dehydration of Castor Oil over NaHSO4/MCM-41 Catalyst Modified by n-Dodecyltriethoxysilane, *Z. Anorg. Allg. Chem.*, 2017, **643**, 772–779.

47 R. Yamazaki, N. Karyu, M. Noda, S. Fujii and Y. Nakamura, Quantitative measurement of physisorbed silane on a silica particle surface treated with silane coupling agents by thermogravimetric analysis, *J. Appl. Polym. Sci.*, 2016, DOI: 10.1002/app.43256.

48 S. Builes, P. Lopez-Aranguren, J. Fraile, L. F. Vega and C. Domingo, Alkylsilane-Functionalized Microporous and Mesoporous Materials: Molecular Simulation and Experimental Analysis of Gas Adsorption, *J. Phys. Chem. C*, 2012, **116**, 10150–10161.

49 A. Cauvel, D. Brunel, F. DiRenzo, P. Moreau and F. Fajula, Functionalization of Y zeolites with organosilane reagents, *Catalysis by Microporous Materials*, 1995, **94**, 286–293.

50 M. R. Nanda, Z. Yuan, W. Qin, H. S. Ghaziaskar, M.-A. Poirier and C. C. Xu, Thermodynamic and kinetic studies of a catalytic process to convert glycerol into solketal as an oxygenated fuel additive, *Fuel*, 2014, **117**, 470–477.

51 G. L. Catuzo, C. Santilli V and L. Martins, Hydrophobic-hydrophilic balance of ZSM-5 zeolites on the two-phase ketalization of glycerol with acetone, *Catal. Today*, 2021, **381**, 215–223.

52 A. L. Maksimov, A. I. Nekhaev, D. N. Ramazanov, Y. A. Arinicheva, A. A. Dzyubenko and S. N. Khadzhiev, Preparation of high-octane oxygenate fuel components from plant-derived polyols, *Pet. Chem*., 2011, **51**, 61–69.

53 L. Li, T. I. Korányi, B. F. Sels and P. P. Pescarmona, Highly-efficient conversion of glycerol to solketal over heterogeneous Lewis acid catalysts, *Green Chem.*, 2012, **14**, 1611–1619.

54 C. X. A. da Silva, V. L. C. Gonçalves and C. J. A. Mota, Water-tolerant zeolite catalyst for the acetalisation of glycerol, *Green Chem.*, 2009, **11**, 38–41.

55 C. Fan, C. Xu, C. Liu, Z. Huang, J. Liu and Z. Ye, Ketalization of glycerol with acetone to o-heterocyclic compounds over ZrO 2-SiO 2 solid acid catalysts, *Heterocycles*, 2012, **85**, 2977–2986.

56 A. Schwanke and S. Pergher, Lamellar MWW-Type Zeolites: Toward Elegant Nanoporous Materials, *Applied Sciences-Basel*, 2018, DOI: 10.3390/app8091636.

